**Proceedings of ASME 2011 5th International Conference on Energy Sustainability &
9th Fuel Cell Science Engineering and Technology Conference
ESFuelCell2011
August 7-10, 2011, Washington, DC, USA**

ESFuelCell2011-54768

DRAFT: MODELING AND EXPERIMENTS OF VOLTAGE TRANSIENTS OF PEM FUEL CELLS WITH THE DEAD-ENDED ANODE

Jason B. Siegel
University of Michigan
Ann Arbor, MI, USA

Anna G. Stefanopoulou
University of Michigan
Ann Arbor, MI, USA

Serhat Yesilyurt
Sabanci University
Istanbul, Turkey

ABSTRACT

The operation of PEM fuel cells (PEMFC) with dead-ended anode (DEA) leads to severe voltage transients due to accumulation of nitrogen, water vapor and liquid water in the anode channels and the gas diffusion layer (GDL). Accumulation of nitrogen causes a large voltage transient with a characteristic profile whereas the amount of water vapor in the anode is limited by the saturation pressure, and the liquid water takes up very small volume at the bottom of the anode channels in the case of downward orientation of the gravity. Here, we present a transient 1D along-the-channel model of PEMFCs operating with periodically-purged DEA channels. In the model, transport of species is modeled by the Maxwell-Stefan equations coupled with constraint equations for the cell voltage. A simple resistance model is used for the membrane to express the permeance of nitrogen and transport of water through the membrane. The model results agree very well with experimental results for the voltage transients of the PEMFC operating with DEA. In order to emphasize the effect of nitrogen accumulation in the anode, we present experimentally obtained cell voltage measurements during DEA transients, when the cathode is supplied with pure oxygen. In the absence of nitrogen in the cathode, voltage remained almost constant throughout the transient. Then, the model is used to determine the effect of oxygen-to-nitrogen feed ratio in the cathode on the voltage transient behavior for different load currents. Lastly, the model is used to show the effect of the small amount of leak from the anode exit on the voltage transient; even for leak rates as low as less than 10 ml/h, nitrogen accumulation in the anode channels is alleviated and the cell voltage remained almost constant throughout the transient.

INTRODUCTION

The complexity of the PEMFC balance-of-plant design is a major drawback that impedes its advance especially in transportation applications. For example, the effective utilization of the on-board-stored fuel requires expensive components and advanced mechatronic solutions. A simpler approach to improve the fuel utilization, once its shortcomings are addressed, is to operate the PEMFC with the DEA by using a simple pressure regulator instead of expensive mass flow controllers [1,2,3]. Major shortcomings of the DEA operation are: first, membrane humidification depends on the humidification and product water from the cathode side; second, accumulation of nitrogen dilutes the concentration of hydrogen in the anode channels insofar as hydrogen cannot reach to reaction sites especially near the exit. Along with nitrogen, water vapor accumulates in the anode as well, partially alleviating the first problem, but contributing to the second one. Accumulation of nitrogen and water vapor in the anode blocks hydrogen transport to portions of the active area near the anode exit. Moreover, especially at high current density and relative humidification in the cathode, accumulation of liquid water in the anode-GDL leads to further adverse conditions that render transport of hydrogen difficult throughout the anode [2,3,4,5,6]. Lastly, hydrogen starvation in the PEMFC operating in the DEA mode leads to degradation of the catalyst support through the carbon-corrosion mechanism [7]. Despite all its adverse conditions, the operation of PEMFCs with DEA is not well understood and a closer look at the transport and degradation mechanisms is necessary.

Here, we present a time-dependent one-dimensional along the channel model of DEA transients of PEMFCs between purge cycles. The proposed model is compared with recent ex-

perimental results [8] and agrees reasonably well with the experimentally measured voltage transients. Both the experiments and model results show that the cell voltage in the DEA mode decreases with time, first slowly then rapidly. Depletion of hydrogen in the anode, which is due to accumulation of nitrogen, leads to a slow decay of the cell voltage immediately after the anode exit is closed. As the accumulation of nitrogen continues, hydrogen concentration becomes almost zero near the exit of the anode channels where the current generation from the anode reaction almost stops. Thus, the local current density in the gradually decreasing active area increases to match the load current and results in increasing cathode over potential and decreasing cell voltage at a faster rate than initially observed at the beginning of the transient.

The time-dependent one-dimensional model presented here is described next followed by details of the numerical implementation and simulation results. The model is first tuned and verified with the flow-through data, then validated with the voltage measurements in the DEA transients presented in [8]. Furthermore, results are presented for the transient simulation results that are performed to study the effects of oxygen-to-nitrogen feed ratio in the cathode and a small-leak rate from the anode exit on the time-dependent cell voltage during transients.

DESCRIPTION OF THE MODEL

Here, the description of the time-dependent 1D model of PEMFCs having DEA transients is presented. In the model, Maxwell-Stefan equations are used to calculate concentrations of the species along the anode and cathode channels, and are coupled with a voltage model to obtain the kinetics of reactions. The model incorporates transport resistances through the gas diffusion layers and the membrane and neglects the transient effects in the direction through the plane. Equations used in the model are detailed next; numerical values of the parameters used in the model are listed in Table 1.

Mass transfer

The Maxwell-Stefan equations are used to model the time-dependent transport of species along the anode and cathode channels:

$$\frac{\partial}{\partial t}(\rho w_i)+\frac{\partial}{\partial z}\left(-\rho w_i\sum_j D_{ij}\frac{\partial x_j}{\partial z}+\rho w_i U\right)=r_i \qquad (1)$$

where w is the mass fraction, x is the mole fraction, ρ is the density, D_{ij} binary diffusion coefficient of species i and j, z is the coordinate in the direction of the flow, t is time, U is the convective velocity and r is the reaction rate: species in the anode channel are H_2, H_2O vapor and N_2, and in the cathode are O_2, H_2O vapor and N_2. The Maxwell-Stefan equations are solved for two species at the anode and cathode; the mole fraction (or the mass fraction) of the third component is determined from the conservation of total mass:

$$x_3 = 1 - x_1 - x_2 \qquad (2)$$

Binary diffusion coefficients in (1) are obtained for multi-component mixtures [9]:

$$D_{ij} = 3.16\times10^{-8}\left(\frac{T^{1.75}}{p\left(v_i^3+v_j^3\right)^2}\right)\left(\frac{1}{M_i}+\frac{1}{M_j}\right)^{1/2} \qquad (3)$$

where p is the pressure, v_i is the molar volume of species i, T is temperature, and M_i is the molecular weight of species, i.

In (1), densities of mixtures in the anode and cathode are obtained from the Dalton's Law:

$$\frac{1}{\rho}=\frac{\sum_i \frac{w_i}{M_i}}{p/(RT)} \qquad (4)$$

where R is the universal gas constant.

The convective velocity, U, in (1) is the average velocity of the flow, and determined from the sum of the velocity that corresponds to the exit stoichiometric ratio of the flow and the total flux of the species reacting at the catalyst layer and exchanged at the membrane:

$$U = U_{exit} + U_{flux} \qquad (5)$$

In the cathode side, the convective velocity is determined from the stoichiometric ratio of the flow, which is usually set to a value sufficiently larger than one. In the anode, the flow of hydrogen, especially near the inlet, is the major part of the convective velocity, since all the hydrogen consumed in the reaction flows through the inlet. The convective velocity due to fluxes of species reacting and crossing over the membrane at a given position is the integral of the mass fluxes downstream when the anode is dead-ended, i.e.:

$$U^{an}_{flux}(z) = -\frac{1}{\rho_{an}}\int_z^L N^{an}_{H_2}(z') + N^{an}_{N_2}(z') + N^{an}_{H_2O}(z')\,dz' \qquad (6)$$

Here, L is the length of the channels, N_i^{an} are the inward mass fluxes across the membrane for water vapor and nitrogen.

The inward mass flux of hydrogen that reacts at the catalyst layer is obtained from:

$$N^{an}_{H_2} = -\frac{M_{H_2}}{2F}\left(J_{cell}+J_{loss}\right) \qquad (7)$$

where F is the Faraday's constant, J_{cell} is the local current density and J_{loss} is the parasitic current density due to the loss of hydrogen that permeates through the membrane to the cathode side. It is assumed that the parasitic loss is proportional to the mole fraction of hydrogen:

$$J_{loss} = J_{loss,0}\,x_{H_2} \qquad (8)$$

where $J_{loss,0}$ is an estimated constant based on the permeance of hydrogen through the Nafion membrane.

The local flux of nitrogen through the membrane is calculated from the difference between the partial pressures of nitrogen in the cathode and the anode:

$$N_{N_2}^{an} = M_{N_2}\psi_{N_2}\frac{p\left(x_{N_2}^{ca} - x_{N_2}^{an}\right)}{\delta_m} \tag{9}$$

Here, δ_m is the thickness of the membrane, and ψ_{N_2} is the membrane-water-content dependent permeance of nitrogen and given by [2]:

$$\psi_{\mathrm{N_2}} = \psi_{\mathrm{N_2}}^0\left(0.0295 + 1.21 f_V - 1.93 f_V^2\right)\exp\left[\frac{E_{\mathrm{N_2}}\left(T - T_0\right)}{RTT_0}\right] \tag{10}$$

where $\psi_{\mathrm{N_2}}^0$ is 1×10^{-14} mole/m^2, $E_{\mathrm{N_2}}$ is 24 kJ/mole and f_V is the volumetric ratio of the liquid water in the membrane, and given by:

$$f_V = \frac{\lambda V_{\mathrm{H_2O}}}{V_m + V_{\mathrm{H_2O}}} \tag{11}$$

Here, λ is the molar ratio of water molecules per sulfonic group in the membrane, V_m and $V_{\mathrm{H_2O}}$ are the molar volumes of the dry membrane and liquid water.

In (6), the flux of water vapor across the membrane is given by:

$$N_{\mathrm{H_2O}}^{an} = M_{\mathrm{H_2O}}\left[\frac{c_{\mathrm{SO_3}}^0\left(\lambda_{eq}^{ca} - \lambda_{eq}^{an}\right)}{R_m} - n_d\frac{J_{cell}}{F}\right] \tag{12}$$

where $\lambda_{eq}^{(an,ca)}$ is the water content of the membrane at the local equilibrium conditions at the anode and cathode; $c_{\mathrm{SO_3}}^0$ is the molar concentration of sulfonic groups in the dry membrane; and n_d is the electro-osmotic drag coefficient that gives the number of water molecules dragged by each proton; and R_m is the membrane's resistance to water flux and given by:

$$R_m = \frac{1}{k_{ads}} + \frac{1}{k_{des}} + \frac{\delta_m}{D_\lambda} \tag{13}$$

In (13), k_{des} and k_{ads} are the desorption and adsorption coefficients and D_λ is the diffusion coefficient of water; k_{des}, k_{ads} and D_λ are experimentally measured by Ge *et al* [10] and given by:

$$k_{des} = 4.59\times10^{-5} f_V \exp\left[2416\left(\frac{1}{T} - \frac{1}{T_0}\right)\right] \tag{14}$$

$$k_{ads} = 1.14\times10^{-5} f_V \exp\left[2416\left(\frac{1}{T} - \frac{1}{T_0}\right)\right] \tag{15}$$

$$D_\lambda = 2.72\times10^{-9} f_\lambda \exp\left[2416\left(\frac{1}{T} - \frac{1}{T_0}\right)\right] \tag{16}$$

where f_λ is temperature dependent and specified as:

$$f_\lambda = \begin{cases} .0543 + .00336\lambda, T = 323\mathrm{K} \\ .0771 + .00259\lambda, T = 353\mathrm{K} \end{cases} \tag{17}$$

On the cathode, the local inward oxygen flux due to the reaction at the catalyst layer is given by:

$$N_{\mathrm{O_2}}^{ca} = -\frac{1}{4F}M_{\mathrm{O_2}}\left(J_{cell} + J_{loss}\right) \tag{18}$$

The local inward flux of water vapor on the cathode is the sum of the opposite of the flux going into the anode and the water coming out from the reaction at the catalyst layer:

$$N_{\mathrm{H_2O}}^{ca} = M_{\mathrm{H_2O}}\left[-c_{\mathrm{SO_3}}^0\frac{\left(\lambda_{eq}^{ca} - \lambda_{eq}^{an}\right)}{R_m} + \left(\frac{1}{2} + n_d\right)\frac{J_{cell}}{F}\right] \tag{19}$$

The nitrogen flux into the cathode is the opposite of the flux going into the anode, which is given by (9).

In the Maxwell-Stefan equations given by (1), reaction rates are determined from the mass flux of each species given by (7), (9) and (12), i.e.:

$$r_i = \frac{N_i}{d_{eff}} \tag{20}$$

where d_{eff} is the effective depth of the anode and cathode channels and defined as the ratio of the total volume available to species, V_{Total}, and the active area of the fuel cell, A_{cell}, i.e.:

$$d_{eff}^{an,ca} = \frac{V_{Total}^{an,ca}}{A_{cell}} \tag{21}$$

The boundary conditions of the Maxwell-Stefan equations in (1) are specified at inlets and outlets of the anode and cathode channels. At the anode inlet, we assume dry hydrogen is supplied during purges as well as dead-ended conditions, i.e.:

$$\text{At at } z = 0: \quad x_{\mathrm{H_2}} = 1, \quad x_{\mathrm{N_2,H_2O}} = 0 \tag{22}$$

Similarly to the anode boundary conditions, at the cathode inlet, mass fractions of the species are specified based on the inlet relative humidity and the pressure. At the anode and cathode exits, fluxes of species are set to the convective-flux-only conditions: i.e. the diffusive fluxes are zero:

$$-\rho_i\sum_{j\neq i}D_{ij}\frac{\partial x_j}{\partial z} = 0 \tag{23}$$

The convective flux at the exit, $\rho w_i U$, is only from the stoichiometric flow of the species at the exit, U_{exit}, as expressed in (5).

The voltage model

Assuming that the anode electrode is kept at ground, the cathode electrode potential is expressed as the loss from the reversible cell potential, V_{rev}, due to potential drop in the membrane, ΔV_m, anode activation, ΔV_{an} , and cathode activation, ΔV_{ca} , as follows:

$$V_e = V_{rev} - \Delta V_{an} - \Delta V_{ca} - \Delta V_m \tag{24}$$

The reversible cell potential is given by:

$$V_{rev} = V_0 + \frac{RT}{2F}\left[\frac{1}{2}\log\left(\frac{c_{\mathrm{O}_2}}{c_{\mathrm{O}_2}^{ref}}\right) + \log\left(\frac{c_{\mathrm{H}_2}}{c_{\mathrm{H}_2}^{ref}}\right)\right] \tag{25}$$

Here, c_i^{ref} refers to reference concentration of species i, V_0 is the open-circuit potential and given by [11]:

$$V_0 = 1.23 - 0.00083\times(T - 298) \tag{26}$$

The anode and cathode activation over potentials in (24) are given by [12]:

$$\Delta V_{an} = \frac{RT}{F\beta_{an}}\operatorname{asinh}\left[\frac{J_{cell}}{i_{0,ref}^{an}}\left(\frac{c_{\mathrm{H}_2}^{ref}}{c_{\mathrm{H}_2}^{CL}}\right)^{\gamma_{\mathrm{H}_2}}\right] \tag{27}$$

$$\Delta V_{ca} = \frac{RT}{F\beta_{ca}}\operatorname{asinh}\left[\frac{J_{cell}}{i_{0,ref}^{ca}}\left(\frac{c_{\mathrm{O}_2}^{ref}}{c_{\mathrm{O}_2}^{CL}}\right)^{\gamma_{\mathrm{O}_2}}\left(\frac{c_{\mathrm{H}^+}^{ref}}{c_{\mathrm{H}^+}^{CL}}\right)^{\gamma_{\mathrm{H}^+}}\right] \tag{28}$$

In (27) and (28), β is the transfer coefficient, γ is the concentration parameter and $i_{0,ref}$ is the reference current density, c_i^{CL} is the concentration of species i in the catalyst layer, and calculated from the concentration of species in the channels, c_i, using the mass transfer resistance of the GDL as follows:

$$c_i^{CL} = c_i - \frac{\delta_{GDL}}{D_{i,\mathrm{N}_2}} N_i \tag{29}$$

where δ_{GDL} is the thickness of the GDL, D_{i,N_2} is the diffusion coefficient of species i and nitrogen, and N_i is the mass flux.

The last term in the parentheses in (28) represents the overpotential due to proton deficiency in the cathode catalyst layer. In the dead-ended operation there is a severe fuel starvation in parts of the cell, and, hence, the cell current diminishes and the oxygen reaction in the cathode stops as well. We assume that the proton concentration in the cathode remains at equilibrium and does not add to the activation loss.

The potential drop in the membrane is due to Ohmic loss:

$$\Delta V_m = \frac{\delta_m}{\sigma_m} J_{cell} \tag{30}$$

where σ_m is the membrane's ionic conductivity and given by an empirical relationship for Nafion membranes [13]:

$$\sigma_m = (-0.326 + 0.514\,\lambda)\exp\left[1268\left(\frac{1}{303} - \frac{1}{T}\right)\right] \tag{31}$$

The cell potential, V_{cell}, at the cathode current collector must be constant, due to the high conductivity of the plate, and can be determined from the current density and the total electric resistance of the solid components including contacts, R_{solid}; the electric resistance can be estimated from the slope of the polarization curve of the cell. The cell potential is obtained from:

$$V_{cell} = V_e - R_{solid} J_{cell} \tag{32}$$

The integral of the current density, J_{cell}, must be equal to the total load current, I_{load}, which is specified as an input in the model, as follows:

$$\int_{A_{cell}} J_{cell}\, dA = A_{cell} J_{load} = I_{load} \tag{33}$$

The unknowns, which are total of six molar fractions (interchangeably mass fractions) of species, x_i (or w_i), current density, J_{cell}, and the cell potential, V_{cell} are obtained from the solution of the Maxwell-Stefan equations for conservation of mass of individual species, conservation of total mass, coupled with the cell potential and current density equations given by (1), (2), (32) and (33) respectively.

NUMERICAL SOLUTION

The Maxwell-Stefan equations subject to voltage model constraints are solved numerically using a commercial finite-element package, COMSOL Multiphysics [14]. The constraint equation given by (24) is represented in the weak form to ensure a full coupling between the voltage model and the Maxwell-Stefan equations. In the finite-element representation, the one-dimensional domain is discretized into 50 linear elements and 301 degrees of freedom.

Prior to simulating the dead-ended exit transient, the steady-state solution is obtained for a flow through operation mimicking the purge-period. In previous experiments, the cell voltage recovered fully during the purge cycles especially for dry operating conditions at the cathode [8]. Therefore, it is assumed that nitrogen and water vapor, which accumulate during the dead-ended transient, are completely removed from the anode channels and GDLs, and that steady-state flow through conditions are almost restored during the purge cycle.

In order to obtain a converged steady-state solution of the non-linear equations with Newton-Raphson iterations, the coupling between the Maxwell-Stefan equations, cell voltage and current constraints is bootstrapped. First the Maxwell-Stefan equations for the anode are solved; then this solution is

coupled with the cathode's Maxwell-Stefan equations; finally, the full set of equations is solved together.

The steady-state solution is used as the initial condition of the dead-ended transient. A variable-step-size maximum third-order backward-difference-formula is used to integrate the discrete system of equations in time with the maximum absolute tolerance of 10^{-4} [14].

Table 1: Model parameters and their values

Parameter	Value
Thickness of the membrane, δ_m	25×10^{-6} m
Effective depth of the anode and cathode channels, $d_{eff}^{\{an,ca\}}$	$\{12.7,4.69\}\times10^{-4}$m
Length of the channels, L	0.073 m
Operation and reference temperatures, T, T_0	333 ve 300 K
Operation and reference pressures, p, p_0	1.25 ve 1 bar
Cathode inlet relative humidity, RH_{ca}	0.6
Cathode inlet stoichiometric ratio	3
Molar volume of the membrane, V_m	0.9×10^{-3} m^3/mole
Concentration of sulfonic groups in the dry membrane, $c_{SO_3}^0$	1200 mole/m^3
Permeance coefficient of N_2, $\psi_{N_2,0}$	1.0×10^{-14} mole/m^2
Reference concentrations of H_2 and O_2, $c_{\{H_2,O_2\}}^{ref}$	{56.4,40} mole/m^3
Electro-osmotic drag coefficient, n_d	$(2.5/22)\times\lambda$
Reference current density at the anode and cathode, $i_{0,ref}^{(an,ca)}$	$\{3\times10^4,6\times10^{-3}\}$ A/m^{-2}
Electric resistance of solid parts, R_{solid}	0.3×10^{-4} Ω-m^2
O_2 concentration coefficient, γ_{O_2}	1
H_2 concentration coefficient, γ_{H_2}	1/2
Anode and cathode transfer coefficients, $\beta_{\{an,ca\}}$	{1,1}
Current loss parameter, $J_{loss,0}$	20 A/m^2

RESULTS

In the model presented here, the cathode reference current density, $i_{0,ref}^{ca}$, and the electric resistance of the solid components, including the contact resistance, R_{solid}, are tuned with the experiments reported in our previous work, [8], from the flow through data of the single cell, which was used in the dead-ended transient experiments. Tuning of the reference current density, which also includes the effect of the catalyst layer, and the electrical resistance is necessary, because theoretical values of those parameters for the materials used in the cell would differ from the actual configuration of the PEMFC used in the experiments. The polarization curve shown in figure 1 verifies the tuning of those parameters in the model.

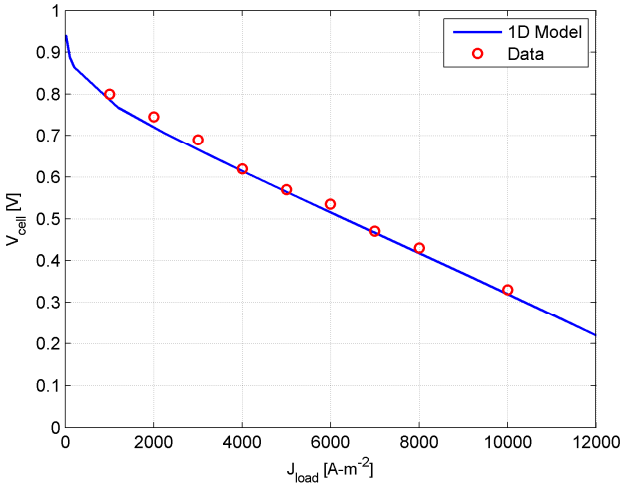

Figure 1: Comparison of the polarization curves from the experiments reported in [8], and the model.

Comparisons of the responses of the cell voltage during DEA transients from the experiments and the simulations are shown in figures 2 and 3 for J_{load} = 3700 and 5700 A/m^2 respectively. The model predicted voltage responses agree reasonably well with the measured voltages in the experiments for both load current densities.

According to results presented in figures 2 and 3, the cell voltage begins to decline at a slow rate up to 400 seconds of the transient, then the rate of voltage decline speeds up. In the previous work, [8,15], it was shown that the slope of the voltage decline increases once the local hydrogen concentration goes to zero near the exit of the anode channel due to nitrogen crossover from the cathode to the anode. The size of the effective active area decreases with the increasing amount of nitrogen in the anode. During the slow ramp-down, the cell voltage drops because of the decreasing hydrogen concentration; and during the fast ramp-down, the voltage drops because of the increasing effective current density only in the portion of the active area where there is sufficient hydrogen for the anode reaction.

In the experiments presented in [8], a solenoid valve downstream from the anode exit is used to close the anode exit. The part of tubing between the actual exit of the anode channels and the valve may act as a reservoir and allow some nitrogen that accumulates in the anode to travel into the available volume in the tubing. In order to mimic the flow of nitrogen into the tubing before the solenoid valve, small leak rates are specified at

the anode exit, 0.23 ml/h (corresponding stoichiometric ratio is 0.0001) for J_{load} = 3700 A/m^2 and 0.17 ml/h (corresponding stoichiometric ratio is 0.00005) for J_{load} = 5700 A/m^2 respectively in the model.

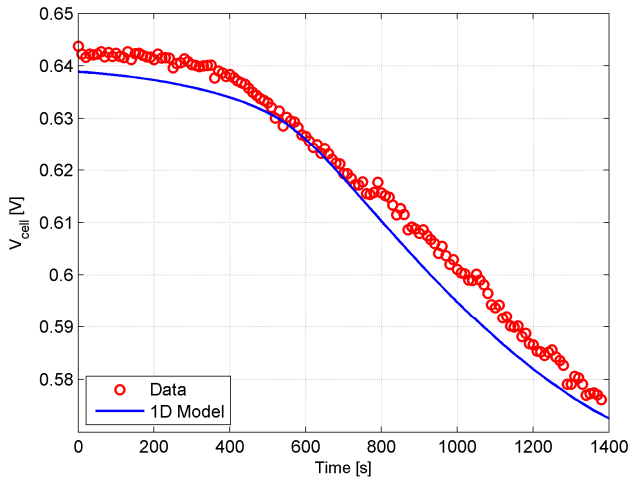

Figure 2: The voltage transient during the dead-ended operation for J_{load} = 3700 A-m^{-2}

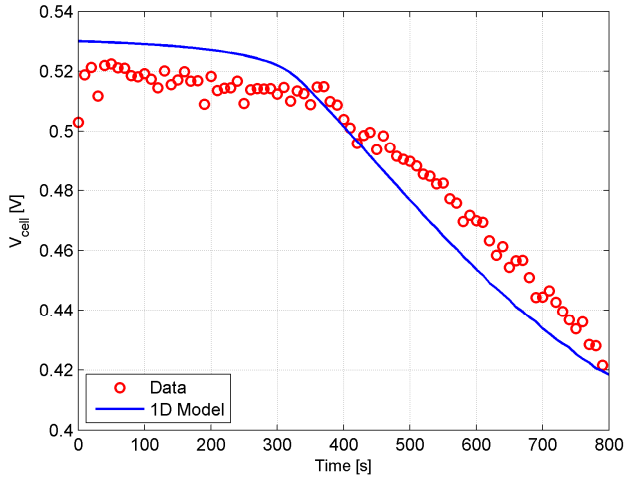

Figure 3: The voltage transient during the dead-ended operation for J_{load} = 5700 A-m^{-2}

The effect of the oxygen-to-nitrogen ratio

The utmost importance of the nitrogen crossover from the cathode to dead-ended anode is demonstrated with experiments, in which air on the cathode side is replaced with pure oxygen. In experiments, an identical cell to the one reported in [8] is used. The cell operated with the load current density of 4000 A/m^2, cathode inlet relative humidity of 0.8 and with the DEA transients that take 2100 seconds between purges. After the initial cycle with a 15 mV drop in the cell voltage, the change of the cell voltage remained within 5 mV in subsequent cycles as shown in figure 4. The cell voltage remained unaffected by dead-ended transients for load current densities 6000 and 8000 A/m^2 as well (not shown here).

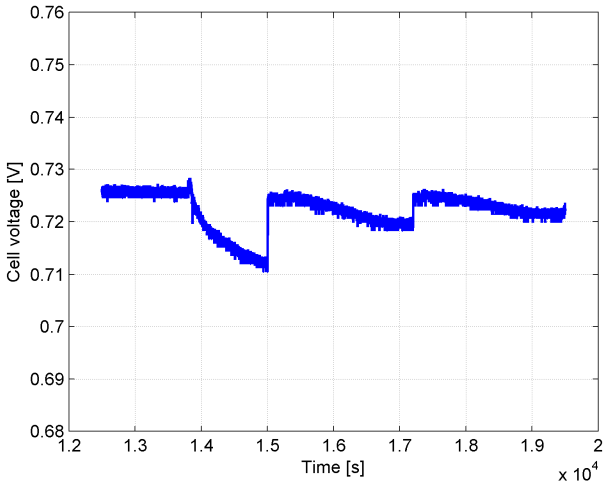

Figure 4: Voltage transient during the dead-ended operation with pure oxygen in the cathode for J_{load} = 4000 A/m^2.

A number of transient simulations are carried out to study the effect of the oxygen-to-nitrogen feed ratio on the cell voltage during the dead-ended operation of the cell. In the simulations, the cathode stoichiometric ratio is set to 3, unless the cathode velocity is below 1 m/s. In figures 5 and 6, the cell voltage transients are shown for a number of oxygen-to-nitrogen ratios in the cathode for J_{load} = 3700 and 5700 A/m^2 respectively. Consistently with the experiments with pure oxygen in the cathode, the cell potential varies very little when the oxygen-to-nitrogen ratio in the cathode is very high. As the ratio is reduced, the double-sloped response of the cell voltage is observed during transients. Furthermore, regardless of the magnitude of the load current, the duration of the slow ramp-down of the cell voltage decreases as the oxygen-to-nitrogen ratio increases.

The effect of the anode exit leak

Transient simulations are carried out with a number of leak rates specified at the anode exit to study their effects. In figure 7, the cell voltage transients are shown for exit leak rates of 0, 0.41, 0.81, 1.63, 2.44, 4.07 and 8.15 ml/h and for J_{load} = 3700 A/m^2. Total drop in the voltage decreases with increasing leak rate from about 90 mV with no leak at the exit to 3.8 mV for a leak rate of 8.15 ml/h, which corresponds to exit stoichiometric ratio of .001 at the anode. In figure 8, for J_{load} = 5700 A/m^2, the exit leak rates are specified as 0, 0.63, 1.26, 3.77 and 6.28 ml/h. The cell voltage drop at the end of 800-second transient is 82 mV when there is no leak, only 7 mV when there is a leak as low as 6.28 ml/h at the exit corresponding to stoichiometric ratio of 0.0005.

According to simulation results shown in figures 7 and 8, the initial response of the cell voltage remains almost identical

for all leak rates. At the beginning of the transient, as long as the leak rate is not too strong, the accumulation of nitrogen in the anode does not vary the distribution of hydrogen insofar as the voltage transient is concerned. As the leak rate increases, discharge of nitrogen accumulated in the anode increases and the rate of decline of the cell voltage decreases.

In order to effectively restore the cell voltage that tends to decline with the accumulation of nitrogen, the leak rate at the anode exit must be high enough to discharge nitrogen from the anode and must be low enough to preserve the fuel and water vapor in the anode. For example, for J_{load} = 3700 A/m^2, assuming that nitrogen concentration is low in the anode, total rate of nitrogen accumulation in the anode is about 3.5 ml/h from a simple calculation using (9) and (10). Thus, clearly, leak rates as low as a few mili-liters-per-hour will be enough to discharge nitrogen and ensure somewhat uniform distribution of hydrogen in the active area.

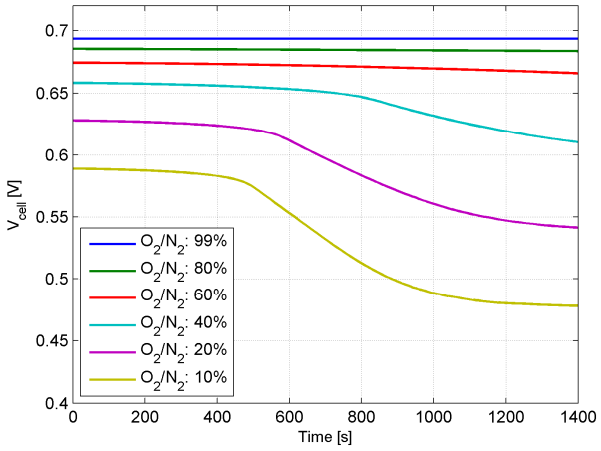

Figure 5: The effect of the O_2/N_2 ratio on the cell voltage during the dead-ended-anode transient for J_{load}=3700 A/m^2.

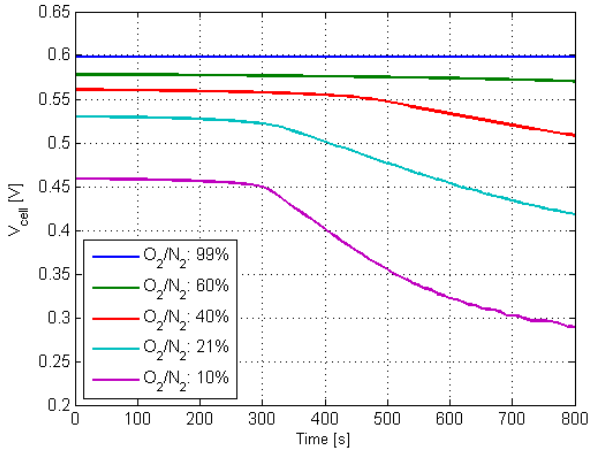

Figure 6: The effect of the O_2/N_2 ratio on the cell voltage during the dead-ended-anode transient for J_{load}=5700 A/m^2.

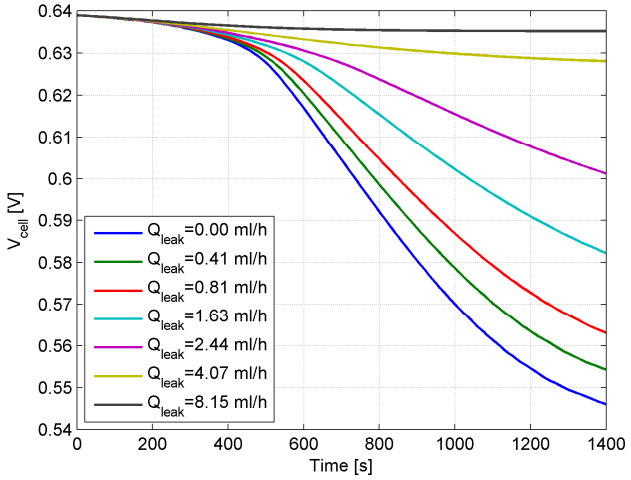

Figure 7: The effect of the anode exit leak on the cell voltage during the dead-ended transients for J_{load} = 3700 A/m^2.

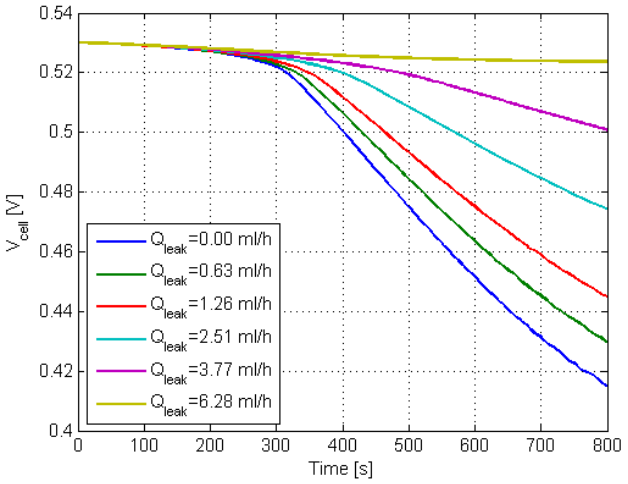

Figure 8: The effect of the anode exit leak on the cell voltage during the dead-ended transients for J_{load} = 5700 A/m^2.

CONCLUSION

The time-dependent one-dimensional (in the flow direction) model of the PEMFC operating with periodically-purged dead-ended anode channels is presented here. For verification and calibration, two parameters of the model are tuned with the flow through experiments of the PEMFC that is used for the dead-ended transient experiments as well: namely, the reference current density in the cathode and the electrical resistance of the solid components including the contact resistance. Then, the verified model is used for dead-ended transients of two load current densities, 3700 and 5700 A/m^2 for validation against experimental results; voltage transients during the DEA operation agree very well with experimental results.

In order to study the effect of nitrogen accumulation in the voltage response during the transients, experiments are conducted with pure oxygen in the cathode. The cell voltage effectively remains unaffected during the DEA transient, confirming the effect of the nitrogen in the voltage decline. Further simulations are carried out in order to study the effect of the oxygen-to-nitrogen ratio in the cathode on the cell voltage during the DEA transient. As the oxygen ratio increased in cathode feed, the cell voltage becomes less responsive during DEA transients.

Lastly, the effect of the anode exit leak (on the order of a few ml/h's) is studied with the model. The simulation results show that a leak rate of less than 10 ml/h is sufficient to discharge the most of accumulated nitrogen from the anode, and to keep the cell voltage nearly flat during the DEA transients.

ACKNOWLEDGMENTS

This work was supported by The Scientific and Technological Research Council of Turkey, TUBITAK-MAG 109M105, and the National Science Foundation through CBET-0932509.

REFERENCES

[1] Karnik, J. Sun, and J. Buckland, 2006, "Control analysis of an ejector based fuel cell anode recirculation system," In Proceedings of American Control Conference, June 2006.

[2] Ahluwalia, R.K, Wang, X., 2007, "Buildup of nitrogen in direct hydrogen polyner-electrolyte fuel cell stacks," *J. Power Sources,* **171**, pp. 63-71.

[3] Muller, E.A., Kolb, F., Guzzela, L., Stefanopoulou, A.G., McKay, D., 2010, "Correlating nitrogen accumulation with temporal fuel cell performance," *J. Fuel Cell Science and Technol.*, **7**(2):021013.

[4] Kocha, S.S., Yang, J.D., Yi, J.S., 2006, "Characterization of gas crossover and its implications in PEM fuel cells," *AICHE Journal*, **52**(5), pp. 1916-1925.

[5] Weber, A.Z., 2008, "Gas-crossover and membrane-pinhole effects in polymer electrolyte fuel cells," *J. Electrochem Soc.*, **155**(6), pp. B521-B531.

[6] Siegel, J.B., McKay, D.A, Stefanopoulou, A.G., Hussey, D.S., Jacobson, D.L., 2008, "Measurement of liquid water accumulation in a PEMFC with dead-ended anode," *J. Electochem. Soc.*, **155**(11), pp. B1168-B1178.

[7] Raiser, C.A., Bregoli, L., Patterson, T.W., Yi, J.S., Yang, J.D., Perry, M.L., Jarvi, T.D., 2005, "A reverse-current decay mechanism for fuel cells," *Electrochem Solid-State Lett.*, **8**(6), pp. A1432-1442.

[8] Siegel, Bohac, S.V., D.A, Stefanopoulou, Yesilyurt, S., 2010, "Nitrogen front evolution in purged polymer electrolyte membrane fuel cell with dead-ended anode" *J. Electochem. Soc.*, **157**(7), B1081-B1093.

[9] Bird, R.B., Stewart, W.E., Lightfoot, E.N., 2002, *Transport Phenomena*, 2nd ed, Wiley, New York.

[10] Ge, S., Li, X., Yi, B., Hsing, I-M., 2005, "Absorption, desorption, and transport of water in polymer electrolyte membranes for fuel cells," *J. Electrochem. Soc.*, **152**(6), A1149-A1157.

[11] Barbir, F., 2005, *PEM Fuel Cells: Theory and Practice*, Academic Press.

[12] Newman, J., Thomas-Alyea K.E., 2004, *Electrochemical Systems,* 3rd ed. John Wiley & Sons, New Jersey, USA.

[13] Springer, T.E., Zawodzinski, T.A., and Gottesfeld, S., 1991, "Polymer electrolyte fuel cell model", J. Electrochem. Soc., 138(8), 2334-2342.

[14] COMSOL, 2010, "COMSOL Multiphysics User Guide," COMSOL A.B., Stockholm.

[15] Siegel J.B., Stefanopoulou, A.G., Yesilyurt, S., 2010, "Modeling and Simulations of PEMFCs Operating with Periodically Purged Dead Ended Anode Channels," In Proc. of the ASME 2010 Eighth International Fuel Cell Science, Engineering and Technology Conference, June 2010.

[16] Benziger, J., Kimball, E., Meija-Ariza, R., Kevrekidis, I., 2010, "Oxygen Mass Transport Limitations at the Cathode of Polymer Electrolyte Membrane Fuel Cells," *AIChE Journal*¸ DOI: 10.1002/aic.12455.